Electronic Supplementary Information (ESI)

# Carbonyl-Enriched Hierarchical Carbon Synergizes Redox Electrolyte for Highly-Efficient and Stable Supercapacitors

Muhammad Imran Rafiq, Xinlei Wang, Tanveer Farid, Jie Zhou, Jian Tang and Weihua Tang*

School of Chemical Engineering, Nanjing University of Science and Technology, Nanjing

210094, People's Republic of China

*Corresponding author:

E-mail:  whtang@njust.edu.cn

# 1. Experimental Section

## 1.1 Chemicals and materials

Balsa wood chips, $CuCl_2$ anhydrous, $HNO_3$, Li-OH, $Cl_2CHCOOH$, and $C_2H_5OH$ were utilized straightforwardly without any extra decontamination.

## 1.2 Preparation of C=O enriched carbon porous leave/carbonized wood hybrid

The dry Balsa wood chips (2.5 cm × 2.0 cm × 1.5 mm, Length × width × thickness) were dipped in 1.5 M solutions of LiOH and $Cl_2CHCOOH$ in deionized water (100 mL). The wood chips enriched by carbonyl and hydroxide groups for 24 hours at 85 $^O$C was then carbonized to 800 °C at a heating rate of 2 °C min$^{-1}$ and calcined for 2 h in the presence of Nitrogen. An evenly black 3D CPL/CW composite used for freestanding electrode was obtained with dimensions (2.0 cm × 1.0 cm × 1.0 mm), which is denoted as CPL/CW.

## 1.3 Preparation of pristine CW substrate

The Balsa wood chip (2.5 cm × 2.0 cm × 1.5 mm, Length × width × thickness) was dipped in water without use of any C=O source. The treated wood chips were then carbonized by adopting the same approach as for C=O enriched CPL/CW. The as-obtained composite was designated as pristine CW substrate.

## 1.4 Characterization

The morphologies of various samples were observed with the aid of scanning electron microscopy (SEM, S-4800, Hitachi, Japan) at an accelerating voltage of 15 kV. The energy-dispersive X-ray spectrometry (EDS) was applied to determine the distributions of different elements. The X-ray diffraction (XRD) spectra were recorded on a Bruker D8 Diffractometer with Cu Kα radiation (1.54 Å) at 40 kV and 30 mA.

The investigation of different elements within the composite was performed by X-ray photoelectron spectroscopy (XPS), in which a Thermo ESCALAB 250X-ray photoelectron spectrometer was utilized with Al Kα radiation (1486.7 eV). The confocal Raman Spectrometer is applied with a 514 nm laser beam and Raman spectra is obtained. The hole volume and superficial area of the CPL/CW and CW were calculated via a Brunauer-Emmet-Teller (BET) surface analyzer (Micrometrics, ASAP 2020).

## 1.4 Electrochemical measurements

CHI 760D electrochemical workstation (Shanghai, China) was used to evaluate the electrochemical performances of electrodes. A stranded three-electrode cell, a platinum foil as the counter electrode, and Ag/AgCl electrode as the reference electrode with 0.06M $CuCl_2$ and 1M $HNO_3$ aqueous electrolyte was used to carry out performance tests of the working electrode. The CPL/CW specimens with the dimension of 2.0 cm × 1.0 cm × 1.0 mm were directly used as free-standing working electrodes.

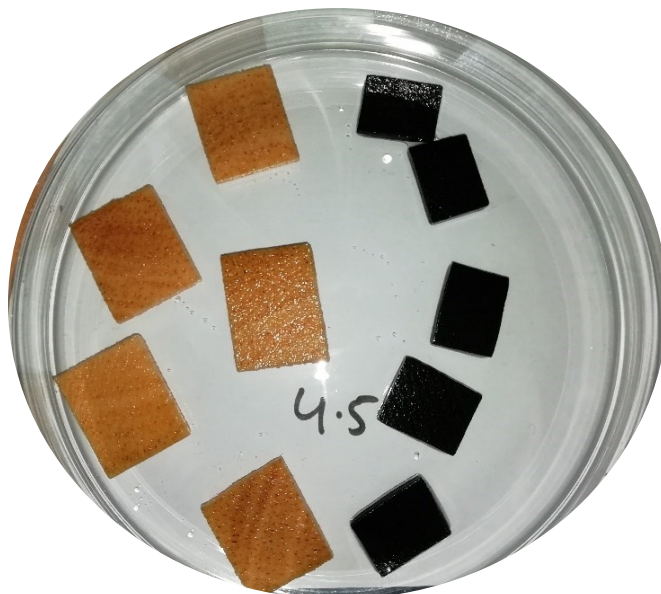## 2. Morphology, porosity and FT-IR analysis



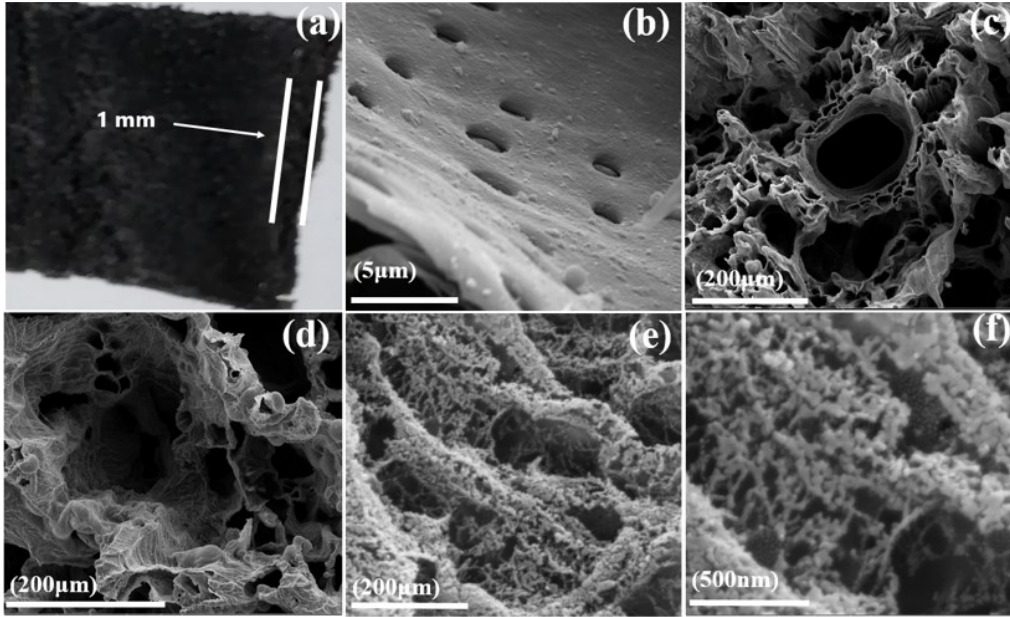**Fig. S1. Optical images for wood and CPL/CW.**

**Fig. S2.** SEM images of CW and CPL/CW (a) CPL/CW freestanding electrode (b) Inner view of CW channel (c) CPL covered all channels of CW (d) CW channels are open after Uniform growth of CPL for ions transportation (e) CPL consists of nano-balls (f) Nano-ball are attached with each other and are in pattern.
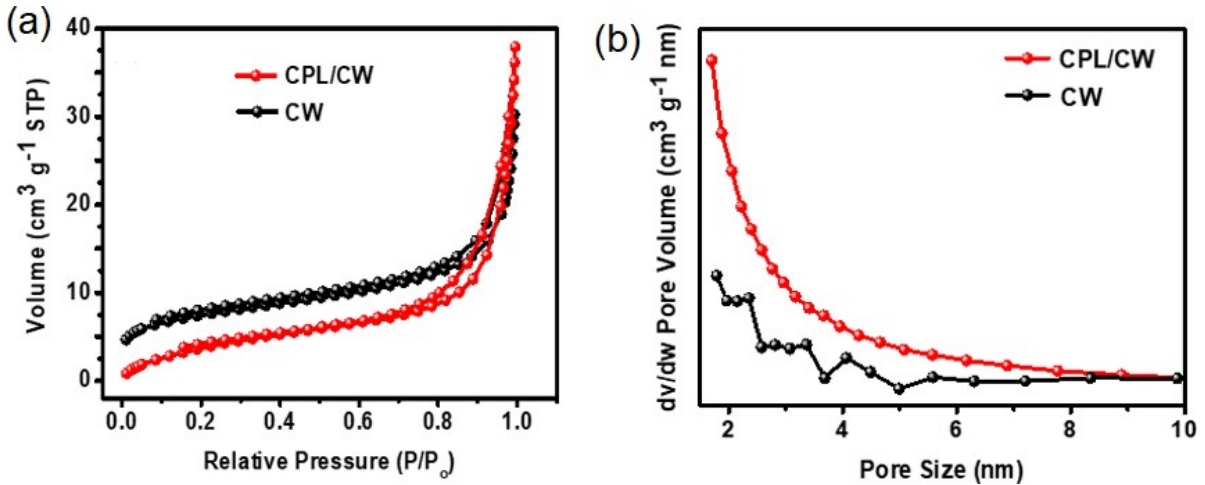


**Fig. S3.** (a) BET surface area of CW and CPL, (b) pore size versus pore volume of CPL/CW and CW
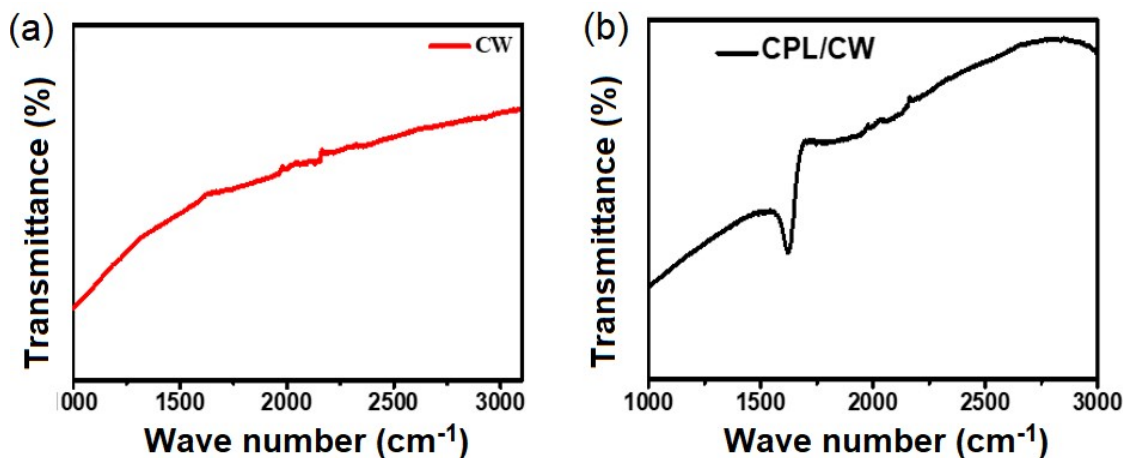
**Fig. S4.** FTIR of spectra of (a) CW and (b) CPL/CW.

## 3. Electrochemistry comparison between CW and CPL/CW
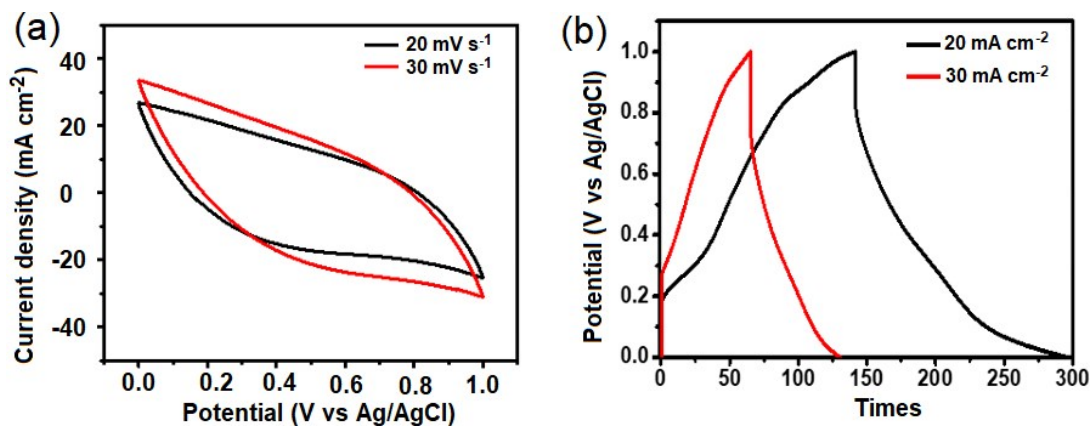


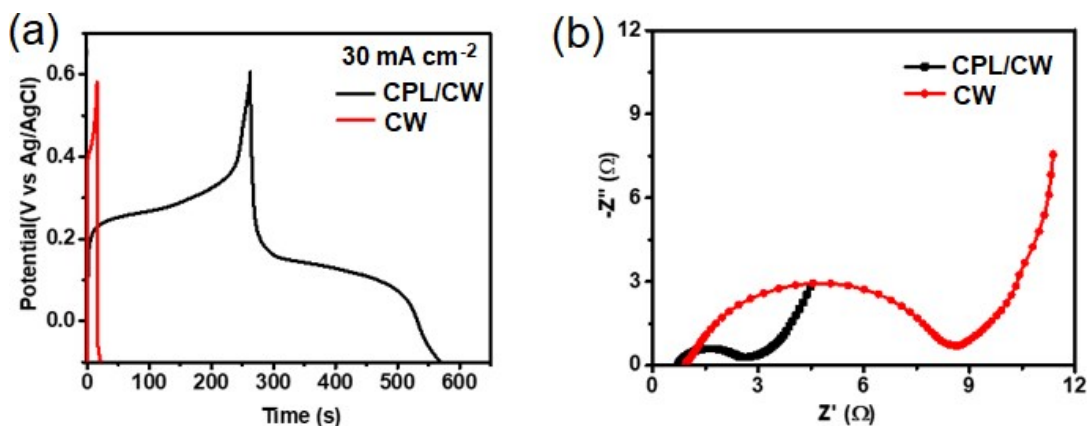**Fig. S5.** Electrochemical performance of CPL/CW in 2 M $HNO_3$ electrolyte (a) CV curves (b) GCD curves.



**Fig. S6.** (a) CV curves and (b) EIS curves for CPL/CW and CW in $CuCl_2$ (0.06 M) $HNO_3$ (1 M) aqueous electrolyte.

# 4. Summary of representative carbon electrodes for high-performance supercapacitors

**Table S1** Specific capacitance comparison of representative carbon-based electrodes for supercapacitors in the literature

| Electrode | Current Density | Capacitance | Ref. |
|---|---|---|---|
| Nitrogen-doped graphene hollow nanospheres | $1\ A\ g^{-1}$ | $381\ F\ g^{-1}$ | [1] |
| hierarchical porous hollow carbon spheres with few-layer graphene framework | $0.5\ A\ g^{-1}$ | $561\ F\ g^{-1}$ | [2] |
| Carbon nanotube balls | $1\ A\ g^{-1}$ | $80\ F\ g^{-1}$ | [3] |
| hollow carbon nanospheres with interconnected mesoporous shells by co-sol-emulsion-gel synthesis | $0.5\ A\ g^{-1}$ | $230\ F\ g^{-1}$ | [4] |
| redox-active electrolyte and binder-free functionalized carbon | $60\ A\ g^{-1}$ | $1331\ F\ g^{-1}$ | [5] |
| Carbon@MnO$_2$ core-shell nanospheres | $2\ mVs^{-1}$ | $252\ F\ g^{-1}$ | [6] |
| N- and O-doped hollow carbonaceous spheres with hierarchical porous structure | $0.2\ A\ g^{-1}$ | $535\ F\ g^{-1}$ | [7] |
| Hierarchical Porous Carbon Frameworks | $0.2\ A\ g^{-1}$ | $682\ F\ g^{-1}$ | [8] |
| Sulfur-doped nanoporous carbon spheres | $0.5\ A\ g^{-1}$ | $405\ F\ g^{-1}$ | [9] |
| Nitrogen-doped two-dimensional porous carbon sheets | $0.5\ A\ g^{-1}$ | $420\ F\ g^{-1}$ | [10] |
| **Carbonyl-enriched carbon porous leaves/carbonized wood** | **$30\ mA\ cm^{-2}$** **($2.64\ A\ g^{-1}$)** | **$13.1\ F\ cm^{-2}$** **($1154.2\ F\ g^{-1}$)** | **This work** |

## 5. Morphology and EDS mapping for electrodes before and after 45000-cycle GCD
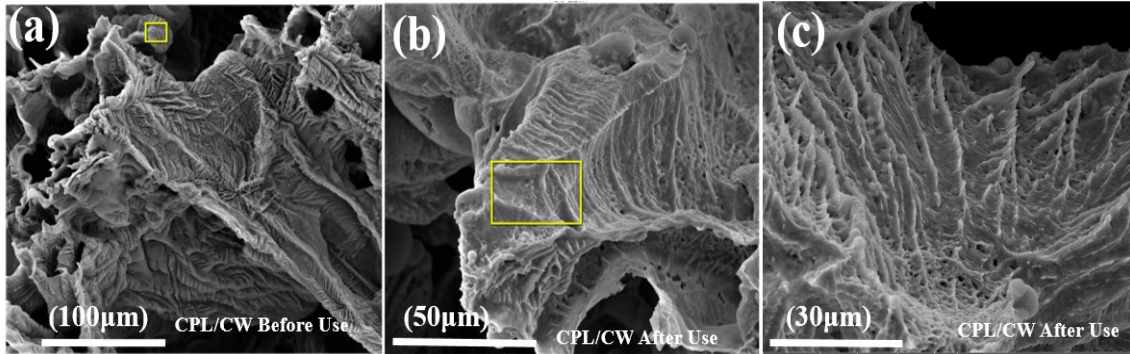


**Fig. S7.** SEM images of CW and CPL/CW (a) CPL/CW before and (b & c) after use.
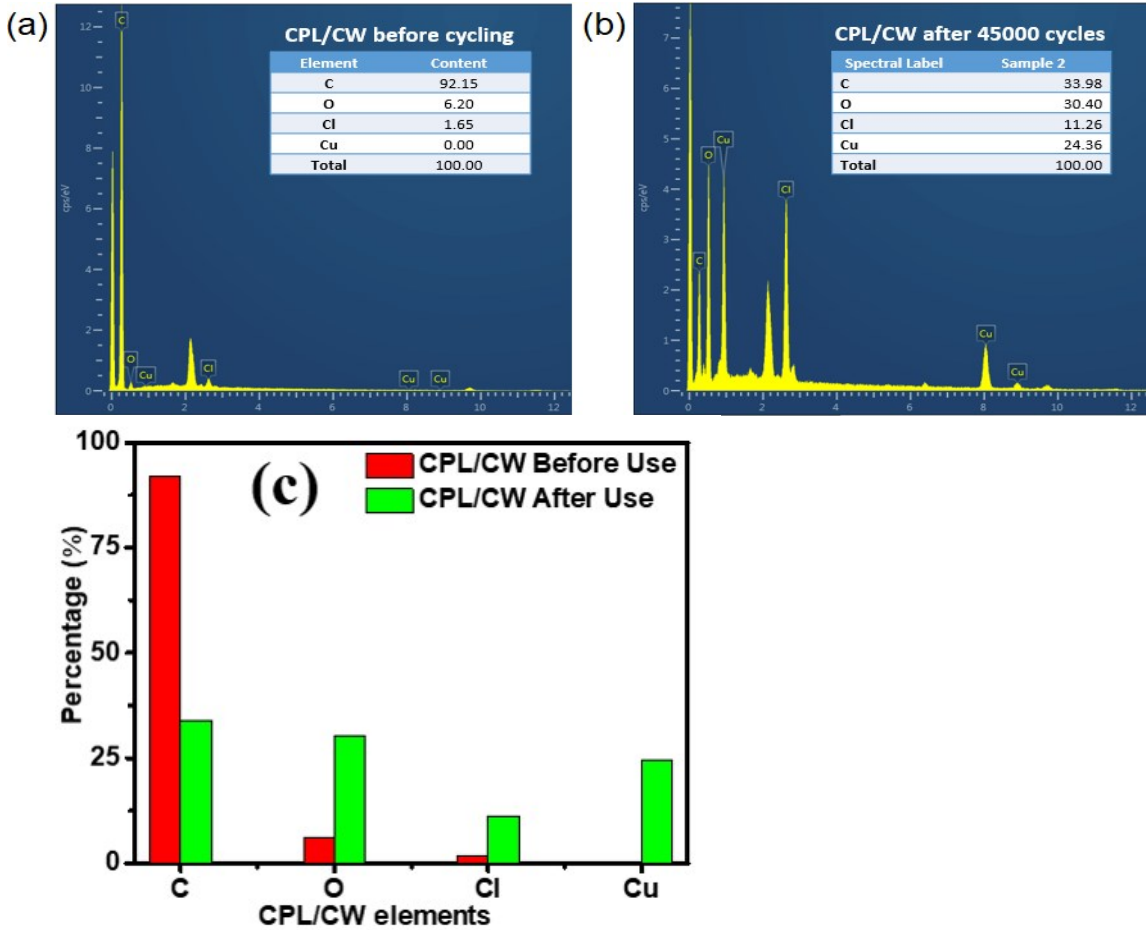


**Fig. S8.** EDX mapping of (a) CPL/CW before and (b) after 45000 cycles. (c) Comparison of elements content change in CPL/CW before and after 45000 cycles.

## References

1   W. Fan, Y. Y. Xia, W. W. Tjiu, P. K. Pallathadka, C. He, and T. Liu, Nitrogen-doped graphene hollow nanospheres as novel electrode materials for supercapacitor applications, *J. Power Sources*, 2013, 243, 973-981.

2   J. Chen, M. Hong, J. Chen, T. Hu, and Q. Xu, Fabrication of hierarchical porous hollow carbon spheres with few-layer graphene framework and high electrochemical activity for supercapacitor, *Appl. Surf. Sci.*, 2018, **443**, 367-373.

3   D. Y. Kang and J. H. Moon, Carbon nanotube balls and their application in supercapacitors, *ACS Appl. Mater. Interfaces*, 2014, **6**, 706-711.

4   J. Hou, T. Cao, F. Idrees, and C. Cao, A co-sol-emulsion-gel synthesis of tunable and uniform hollow carbon nanospheres with interconnected mesoporous shells, *Nanoscale*, 2016, **8**, 451-457.

5   L. Q. Mai *et al.*, Synergistic interaction between redox-active electrolyte and binder-free functionalized carbon for ultrahigh supercapacitor performance, *Nat. Commun.*, 2013, **4**, 3923.

6   Y. Zhao, Y. Meng, and P. Jiang, Carbon@$MnO_2$ core-shell nanospheres for flexible high-performance supercapacitor electrode materials, *J. Power Sources*, 2014, **259**, 219-226.

7   Z. Chen, R. Cao, Y. Ge, Y. Tu, Y. Xia, and X. Yang, N- and O-doped hollow carbonaceous spheres with hierarchical porous structure for potential application in high-performance capacitance, *J. Power Sources*, 2017, **363**, 356-364.

8   C. Chang, H. Wang, Y. Zhang, S. Wang, X. Liu, and L. Li, Fabrication of hierarchical porous carbon frameworks from metal-ion-assisted step-activation of biomass for supercapacitors with ultrahigh capacitance, *ACS Sustain. Chem. Eng.*, 2019, **7**, 10763-10772.

9   S. Liu *et al.*, "Sulfur-doped nanoporous carbon spheres with ultrahigh specific surface area and high electrochemical activity for supercapacitor," *J. Power Sources*, 2017, **360**, 373-382.

10  C. Wang, D. Wu, H. Wang, Z. Gao, F. Xu, and K. Jiang, Nitrogen-doped two-dimensional porous carbon sheets derived from clover biomass for high performance supercapacitors, *J. Power Sources*, 2017, **363**, 375-383.